PAPER Nr. : 63

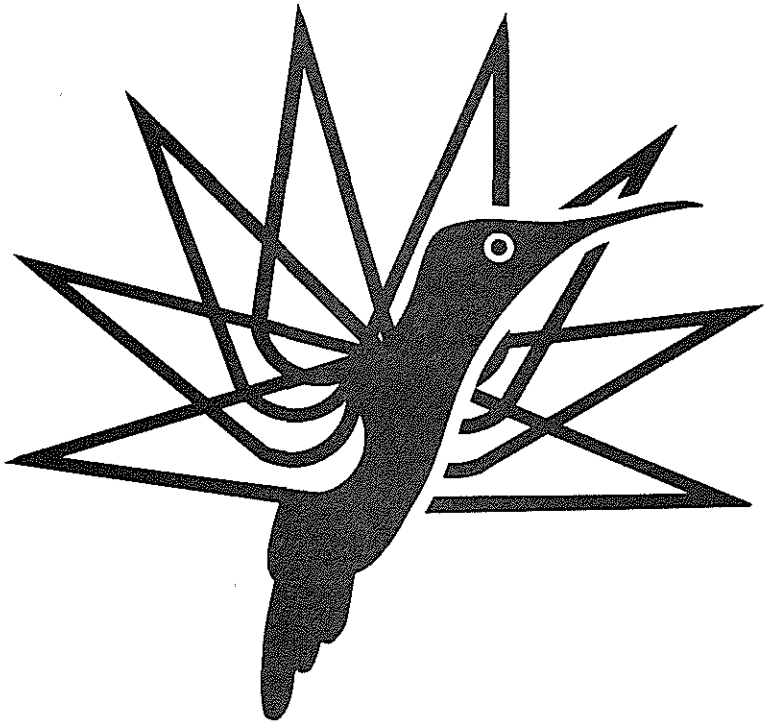

BLADE SECTION DESIGN TO REDUCE ROTOR ROTATIONAL NOISE

by

Yoshiya Nakamura
Assistant, Institute of Industrial Science
Co-Researcher, Institute of Space and Aeronautical Science
University of Tokyo
Tokyo, Japan

FIFTH EUROPEAN ROTORCRAFT AND POWERED LIFT AIRCRAFT FORUM
SEPTEMBER 4 – 7TH 1979 - AMSTERDAM, THE NETHERLANDS

BLADE SECTION DESIGN TO REDUCE ROTOR ROTATIONAL NOISE

Yohsiya Nakamura

Institute of Industrial Science, University of Tokyo

SUMMARY

A new concept of airfoil design to reduce the rotor rotational noise and a numerical method to compute the rotational noise of the rotor blade having arbitrary airfoil section have been developed. The rotational noise composed of monopole noise, dipole noise, and quadrupole noise were calculated for an arbitrary airfoil section at a given angle of attack. The relation between the chordwise source intensity distribution and the computed waveform was studied and the basic concept of low noise airfoil design by shifting the phase of waveform of each noise component, or by changing the source distribution was investigated. So far as monopole and dipole are concerned, it is recommended to make a flat-top lift distribution because the big negative peak of monopole noise might be canceled by the delayed positive peak of dipole noise in waveform.

1 INTRODUCTION

In these years, the mechanism of noise generation of helicopter rotor noise has been studied and many approaches to predict the noise characteristics have been tried. Our next interest is to develop a technique to reduce the noise level which needs the knowledge of the generation mechanism of rotor noise. Some methods of noise reduction were proposed. Tip shape modification was one of the successful methods. Ogee tip, swept back tip, and tapered tip are effective to weaken the intensity of tip vortex, and thus the blade-vortex interaction noise. The swept back tip has become adopted for the new model of production type helicopter. Making big rotor rotate slowly or adopting a small thickness ratio airfoil are other ways of noise reduction, but they have limitations based on the structural stiffness or other design parameters. In the present paper, a new concept of blade sectional shape or airfoil design to reduce the rotor rotational noise and a numerical method to compute the rotational noise of the rotor with arbitrary airfoil section have been developed. In our previous method[1], the noise source was limited to the blade thickness noise and the blade section was assumed to be longitudinally symmetrical, however the computational time was considerably saved because the integration was performed semi-analitically on the rotor fixed coordinates and the numerical time differenciation was replaced by the analytic one. In the present method, the rotor rotational noise composed of thickness noise (acoustic monopole source), loading noise (dipole), and turbulance noise (quadrupole) can be calculated for an arbitrary airfoil section and angle of attack distribution. The angle of attack distribution over the rotor disk was computed by the Local Momentum Theory[2] and the pressure distribution over the blade surface was calculated by the potential theory.

The intensity distribution of each noise source correlates strongly with the observed acoustic waveforms of each noise component, whereas the intensity distributions are related to the blade sectional shape. Then after clarifying these relations completely it must be possible to design a low noise airfoil section by shifting the phase of waveform of each noise component as well as by minimizing the level of each component independently.

NOMENCLATURE

B	number of blades
C	attenuation factor in Local Momentum Theory which means the attenuating rate of induced velocity in the rotor wake
c_0	sound speed
c_h	chord length
c_T	thrust coefficient
c_l	lift coefficient
h	blade thickness distribution function
$I_{1,2,4}$	integrated value of noise source (see eq. (3))
M_n	normal component to the blade surface of local Mach number
m	maximum thickness position as a fraction of chord length
n_j	unit vector normal to blade surface
P_{ij}	stress tensor on the blade surface
p	acoustic pressure
p_1	acoustic pressure of monopole noise
p_2	acoustic pressure of dipole noise
p_4	acoustic pressure of quadrupole noise
p_b	pressure distribution on the blade surface
R	rotor radius
R_0	rotor cut out radius
r_i	vector from source to observer
$\hat{r}_i$	unit vector from source to observer (in other word, propagating direction)
$S_{1,2,4}$	source intensity (see eq. (4))
T	coordinate transfer matrics from the space fixed coordinate to the blade fixed coordinate (see eq. (11))
T_{ij}	Lighthill's stress tensor (see eq. (2))
t	observer time
V_i	aircraft forward velocity vector
v_i	local velocity vector of blade element
x_i	observer position vector
y_i	source position vector
α	angle of attack
β	observer directional angle relative to the moving direction of aircraft
δ	observer elevation angle relative to the rotor plane ($\delta>0$ above the rotor)
ε	blade thickness angle (see eq. (9))
η_i	blade fixed coordinate
θ	blade pitch angle

Λ . . . . directivity parameter (see eq. (5))
μ . . . . advance ratio
ρ_0 . . . . density of atmosphere
σ . . . . solidity
τ . . . . source time
ϕ . . . . blade twist angle
ψ . . . . blade azimuthal angle
Ω . . . . rotor rotational speed

SUBSCRIPT

$( )^T$ . . . matrics transposed
$( )_\eta$ . . . blade fixed coordinate
$( )_x$ . . . space fixed coordinate
$(\vec{\ })$ . . . vector
$(\hat{\ })$ . . . unit vector
$( )_u$ . . . blade upper surface
$( )_l$ . . . blade lower surface
$( )_L$ . . . leading edge position
$( )_T$ . . . trailing edge position
$( )_m$ . . . maximum thickness position

2 BASIC EQUATIONS

By applying a well known Ffawcs Williams and Hawking's equation to helicopter rotor, the following solution of acoustic pressure can be obtained as a function of observer time and position:

$$p(\vec{x},t) = p_1(\vec{x},t)+p_2(\vec{x},t)+p_4(\vec{x},t) \tag{1}$$

$$\left.\begin{aligned} 4\pi p_1 &= \frac{\partial}{\partial t} I_1 \\ 4\pi p_2 &= \frac{\partial}{\partial t} I_2 \\ 4\pi p_4 &= \frac{\partial^2}{\partial t^2} I_4 \end{aligned}\right\} \tag{2}$$

$$\left.\begin{aligned} I_1 &= \int_{R_0}^{R}\int_{\psi_T}^{\psi_L} S_1 \eta_2 d\psi d\eta_2 \\ I_2 &= \int_{R_0}^{R}\int_{\psi_T}^{\psi_L} S_2 \eta_2 d\psi d\eta_2 \\ I_4 &= \int_{-\infty}^{\infty}\int_{R_0}^{R}\int_{\psi_T}^{\psi_L} S_4 d\psi d\eta_2 d\eta_3 \end{aligned}\right\} \tag{3}$$

$$\left.\begin{aligned} S_1 &= \begin{cases} \rho_0 c_0 \vec{v}\cdot\vec{n}_u/(r\Lambda_u) \\ \rho_0 c_0 \vec{v}\cdot\vec{n}_l/(r\Lambda_l) \end{cases} \\ S_2 &= \begin{cases} p_{bu}\vec{n}_u\cdot\hat{r}/(r\Lambda_u) \\ p_{bl}\vec{n}_l\cdot\hat{r}/(r\Lambda_l) \end{cases} \end{aligned}\right\} \tag{4}$$

$$S_4 = T_{ij}\hat{r}_i\hat{r}_j/r\Lambda c_0^4$$

$$\Lambda = \begin{cases} (1+M_{nu}^2-2M_{nu}\vec{n}_u\cdot\vec{\hat{r}})^{1/2} \\ (1+M_{n1}^2-2M_{n1}\vec{n}_1\cdot\vec{\hat{r}})^{1/2} \end{cases} \quad (5)$$

$$M_n = \vec{v}\cdot\vec{n}/c_0 \quad (6)$$

$$\vec{v} = (\eta_2\Omega+V_1\sin\psi-V_2\cos\psi,0,V_3)_\eta^T \quad (7)$$

$$\left.\begin{aligned} \vec{n}_u &= (\sin(\varepsilon_u-\theta-\phi),0,\cos(\varepsilon_u-\theta-\phi))_\eta^T \\ \vec{n}_1 &= (\sin(\varepsilon_1+\theta+\phi),0,-\cos(\varepsilon_1+\theta+\phi))_\eta^T \end{aligned}\right\} \quad (8)$$

$$\varepsilon = \tan^{-1}(\partial h/\partial\eta_1) \quad (9)$$

$$\left.\begin{aligned} r &= |\vec{r}| \\ \vec{r} &= \vec{x}-\vec{y} \\ \vec{\hat{r}} &= \vec{r}/r \\ \vec{\hat{x}} &= (\cos\delta\cos\beta,\cos\delta\sin\beta,\sin\delta)_x^T \end{aligned}\right\} \quad (10)$$

$$(\vec{\ })_\eta = \begin{pmatrix} -\sin\psi,\cos\psi,0 \\ \cos\psi,\sin\psi,0 \\ 0\ ,\ 0\ ,1 \end{pmatrix} (\vec{\ })_x \quad (11)$$

The geometric relations between blade position and the acoustic sphere are shown in Figure 1. The acoustic pressure of each noise component, p, can be obtained by the time differentiation of the integrated value, I, of each noise source, S, located on the blade surface at the retarded time. The influential surface is deformed from the original blade shape by the effect of the rotor rotation or the aircraft movement. The pressure distribution on the blade surface of an arbitrary airfoil section, P_b, may be obtained by a two-dimensional potential theory, for example Moriya's Method for a given angle of attack. This is a dipole noise source whose axis is normal to the blade surface, inward normal for a positive pressure ($P_b>0$), and outward normal for a negative pressure ($P_b<0$). The noise component along the propagating direction (the direction of observer position relative to the source position) of this dipole source vector gives the source intensity. An example of dipole source is shown in Figure 2.

In the past calculation of rotor rotational noise, it has been often assumed that the directivity parameter of the upper surface of the blade, Λ_u, and the lower surface of the blade, Λ_l, are equal. In the present method, however, the solution of acoustic pressure was derived with careful attension to the dependence of source intensity, S, or the directivity parameter,

Λ, or the location of noise source, i.e. whether it locates on the upper surface of the blade or the lower surface. Shown in Figure 3 is an example of comparison of two computing methods, in which more than 20% error in pressure amplitude for a rotor having NACA 0010 airfoil can be observed. It is thus recommended that the directivity parameter, especially for a rotor having airfoils of large twist, camber, or thickness ration like a propellar or comparessor blade shall be estimated precisely.

The angle of attack distribution on the disk, which was calculated by the Local Momentum Theory[2], is shown in Figure 4. The apparent effect of the tip vortex of the former blade on the angle of attack distribution can be seen.

3 GENERAL RELATIONS BETWEEN CHORDWISE SOURCE INTENSITY DISTRIBUTION AND ACOUSTIC WAVEFORM

The solution of acoustic pressure, from equation (1) to (4), can be denoted in a general form as follows:

$$p \sim \frac{\partial}{\partial t} \int_{R_o}^{R} \int_{\psi_T}^{\psi_L} S \eta_2 \, d\psi \, d\eta_2 \sim \frac{\partial}{\partial t} \int_{\psi_T}^{\psi_L} S \, d\psi . \qquad (12)$$

The boundary of the integral is limited by the azimuthal angles of the leading edge, ψ_L, and the trailing edge, ψ_T, at a retarded time. The azimuthal angle, ψ, at the retarded time for a given position on the blade (η_1, η_2) sutisfies the following relation, which can be obtained from geometrical insight shown in Figure 5:

$$\cos\delta(\eta_2 \cos\psi - R)\Omega / (c_o - V_1) + \psi - (\Omega t + 2\pi(i-1)/B - \eta_1/\eta_2) = 0 . \qquad (13)$$

under the condition of $\beta=0$, and $r \gg R$. Substituting $\psi=\psi_L$ or $\psi=\psi_T$, and $i=0$ into equation (13) yields

$$\left.\begin{aligned} &\cos\delta(\eta_2 \cos\psi_L - R)\Omega / (c_0 - v_1) + \psi_L - \Omega t = 0 \\ &\cos\delta(\eta_2 \cos\psi_T - R)\Omega / (c_0 - V_1) + \psi_T - (\Omega t - c_h/\eta_2) = 0 . \end{aligned}\right\} \qquad (14)$$

Since ψ_L and ψ_T are the function of t, the order of differentiation and the integration in the relation (12) is commuted as

$$p \sim \int_{\psi_T}^{\psi_L} \left.\frac{\partial S}{\partial t}\right|_{\psi} d\psi + S(\psi_L)\frac{\partial \psi_L}{\partial t} - S(\psi_T)\frac{\partial \psi_T}{\partial t} \qquad (15)$$

where

$$\left.\frac{\partial S}{\partial t}\right|_{\psi} = \left.\frac{\partial S}{\partial t}\right|_{\psi} + \frac{\partial S}{\partial \eta_1}\left.\frac{\partial \eta_1}{\partial t}\right|_{\psi} . \qquad (16)$$

When a source is in steady state, the first term in the right hand side of the relation (16) can be discarded or $\partial S/\partial t|_{\psi}=0$. By substituting $\partial \eta_1/\partial t = \eta_2 \Omega$, and $\partial S/\partial t|_{\psi}=0$, equation (16) becomes

$$\left.\frac{\partial S}{\partial t}\right|_{\psi} = \eta_2 \Omega \frac{\partial S}{\partial \eta_1} = \frac{\eta_2 \Omega}{c_h} \frac{\partial S}{\partial \hat{\eta}_1} \tag{17}$$

Here, let us consider four typical chordwise source intensity distribution models shown in Figure 6(a) by solid line. Model I and model II show rectangular and triangular lift distribution respectively and model III and model IV show symmetrical double parabolic airfoil section and double parabolic airfoil section of arbitrary position of maximum thickness respectively. The broken lines are chordwise derivatives of the source intensity, $\partial S/\partial \hat{\eta}_1$. From equations (15)~(17) and Figure 6, the acoustic pressures of each model can be obtained as an implicit function of time,

$$\text{I} \quad p \sim \frac{\partial \psi_L}{\partial t} - \frac{\partial \psi_T}{\partial t} \tag{18a}$$

$$\text{II} \quad p \sim \frac{-2\eta_2 \Omega}{c_h}(\psi_L - \psi_T) + 2\frac{\partial \psi_L}{\partial t} \tag{18b}$$

$$\text{III} \quad p \sim \frac{-2\eta_2 \Omega}{c_h}(\psi_L - \psi_T) + \frac{\partial \psi_L}{\partial t} + \frac{\partial \psi_T}{\partial t} \tag{18c}$$

$$\text{IV} \quad p \sim \frac{-\eta_2 \Omega}{2c_h}\left(\frac{\psi_L - \psi_m}{m^2} + \frac{\psi_m - \psi_T}{(1-m)^2}\right) + \frac{\partial \psi_L/\partial t}{2m} + \frac{\partial \psi_T/\partial t}{2(1-m)} \tag{18d}$$

where $\partial\psi/\partial t$ is derived from equation (14) as

$$\frac{\partial \psi}{\partial t} = \Omega / \left(1 - \frac{\eta_2 \Omega}{c_0 - V_1} \sin\psi\right) \quad . \tag{19}$$

Azimuthal angle, ψ, and its time derivative, $\partial\psi/\partial t$, at retarded time are implicit functions of time given by equation (14) and (19). After some numerical calculation, these values at leading edge, ψ_L and $\partial\psi_L/\partial t$, and at trailing edge, ψ_T and $\partial\psi_T/\partial t$, and $\psi_L - \psi_T$ are obtained as a function of time as shown in Figure 7. The time difference of the positive peak of $\partial\psi_L/\partial t$ and $\partial\psi_T/\partial t$ which are caused by the elongation of integral area can be obtained as follows:

$$\frac{\partial}{\partial \psi}\left(\frac{\partial \psi}{\partial t}\right) = \frac{\eta_2 \Omega^2 \cos\psi}{(c_0 - V_1)\left[1 - \eta_2 \Omega \sin\psi / (c_0 - V_1)\right]^2} \tag{20}$$

We can see from the above equation that $\psi = \pi/2$ gives the positive peak of $\partial\psi/\partial t$. By substituting $\psi = \psi_T = \pi/2$, $t = t_L$, $\eta_1 = 0$ and $\psi = \psi_T = \pi/2$, $t = t_T$, $\eta_1 = c_h$, the following equations can be derived:

$$\begin{cases} -R\Omega / (c_0 - V_1) + \pi/2 - \Omega t_L = 0 \\ -R\Omega / (c_0 - V_1) + \pi/2 - \Omega t_T + c_h/\eta_2 = 0 \end{cases} \tag{21}$$

Then the time difference, Δt_{c_h}, is given as

$$\Delta t_{c_h} = t_L - t_T = c_h / \eta_2 \Omega \quad . \tag{22}$$

By superposing curves drawn in Figure 7 according to the equations (18 a~d), the acoustic waveforms of the respective

source distribution in Figure 6(a) are obtained as shown in Figure 6(b). Model I (rectangular) is the most basic model because arbitrary shape of distribution of source intensity can be modeled by successive sum of rectangular pulse. Then the waveform of any model can be given by superposing waveforms of this type, considering the phase delay associated with the chordwise distance between the partitioned pulse position and the leading edge. An assymmetric waveform of this rectangular source model can be explained analytically as follows; the first term in the right hand side of the relation (15) was discarded owing to $\partial S/\partial \hat{\eta}_1|_{\psi=0}$, and the second and the third terms have the same absolute value but opposite sign.

Model II shows a typical lift distribution featured by suction effect at the leading edge. This effect appeared as big positive peak in waveform based on the second term in equation (15) or (18 b). The waveform of model III shows a typical thickness noise waveform featured by big negative peak with two positive peaks in both sides. When the maximum thickness is positioned at mid-chord the waveform may be symmetric as in the case of model III, but when it approaches to the leading edge, the first positive peak becomes bigger than that of the second peak as shown by model IV.

After studying these general relations between source distributions and waveforms, the waveform of any kind of distribution will be predicted by physical insight.

3 DESIGN OF LOW NOISE AIRFOIL SECTION

In the previous section, the relation between four typical models of chordwise source intensity distribution and the respective waveforms were discussed, where it was shown that the strong correlation between the source distribution and the waveform existed. As stated before, the rotational noise of a helicopter consists of monopole noise, dipole noise and quadrupole noise, and the total acoustic pressure is obtained by summing up these components. Then it may be able to find the way to reduce rotational noise by shifting the phase of waveform of each noise component, or by shifting the chordwise source distribution. That is to say, in the ideal extreme, when the summed up source intensity is equal to zero over the rotor blade, the noiseless rotor will be produced.

But in the actual case, the source distribution of monopole and dipole cannot cancel each other. Figure 8 shows an example of source distribution for NACA 0010 airfoil. It can be seen that the dipole source distribution depends strongly on the angle of attack. Besides, the dipole changes its sign according to the observer's position. Considering these facts, it seems to be impossible to design a low noise airfoil of a rotor producing an arbitrary thrust for an observer located at an arbitrary position by the concept of "phase-shift."

But actually we are interested in fly-over noise, which means the observer locates under the rotor ($\delta<0$), and also we know that the observed noise is dominated by the source distributed on the surface near the tip of approaching blade especially right in front of the observer ($\psi=\pi/2$). This means that the angle of attack at $\psi=\pi/2$ and adequate span position near tip can be a representative of a distributed angle of attack. As it is sufficient to consider the noise under these consitions, the concept of "phase-shift" is effective in noise reduction.

Let us check the levels of each source intensity, because if their magnitudes are quite different, canceling effect cannot be expected. From equation (4), the order of intensity of monopole source and dipole source can be checked as

$$r\Lambda S_1 \fallingdotseq 2\rho_0 c_0 v(\partial h/\partial \eta_1) \tag{23a}$$

$$r\Lambda S_2 \fallingdotseq \Delta p_b \cos\delta = (1/2)\rho_0 v^2 C_1 \cos\delta \tag{23b}$$

where

$$v=\eta_2\Omega + V_1 \sin\psi \ .$$

Then the ratio of two kinds of source intensity is given as

$$S_1/S_2=\frac{2\rho_0 c_0 v(\partial h/\partial \eta_1)}{(1/2)\rho_0 v^2 C_1 \cos\delta}=\frac{4(\partial h/\partial \eta_1)}{MC_1\cos\delta} \tag{24}$$

where M is a local Mach number. The ratio of chordwise integral of these two sources is given as

$$\frac{\int_0^m S_1 d\hat{\eta}_1}{\int_0^m S_2 d\hat{\eta}_1}=\frac{\text{thickness ratio}}{MC_1\cos\delta(m/2)} \fallingdotseq 1 \tag{25}$$

where m is the position of maximum thickness as a fraction of chord length. Then it can be said that the order of the source intensity of monopole and dipole is nearly equal.

The monopole source distribution is featured basically by the following characters: (1) a big positive value at the leading edge; (2) zero at the maximum thickness position; (3) a moderately negative value in the rear part of the airfoil. As it is impossible to change these basic characters of monopole distribution, we must improve mainly the dipole distribution by adopting adequate distribution of thickness and camber or leading edge radius to cancel the monopole distribution as follows. (1) To cancel the big positive value of monopole at the leading edge, the big negative value of dipole source around this area is desired. This distribution is obtained by taking a high angle of attack. (2) To cancel the moderate negative value of monopole in the rear part, the positive dipole in this area is disirable.

They are corresponding to the following phenomena in the waveform. By seeing the right hand side of Figure 3, it can be said that the general features of each waveform are: (1) mono-

pole: first positive peak followed by big and steep negative peak and moderate recovering to the second small positive peak; (2) dipole: positive peak just after the first positive monopole peak, zero at the time near the negative monopole peak, and negative peak before the second monopole positive peak. Then it is desirable to shift the whole dipole waveform rearwards to cancel the big negative monopole peak with the positive dipole peak, which is corresponding to the rear part of airfoil sharing high lift or to the flat-top lift distribution.

Of course, each source intensity must be decreased. And also the source concentration must be avoided as much as possible because it will produce a big peak in the waveform by a locally elongating effect in the retarded time integration.

By considering these facts, it is desirable to adopt a thin airfoil to avoid a sudden increase in thickness in the case of monopole noise, and to realize a uniform lift distribution in the case of dipole noise.

5 EXAMPLES OF COMPUTED RESULTS

Figure 9 shows the extreme example of the relation of chordwise source distribution and the observed waveform in the case of thickness noise. The intense source at the leading edge produced by the blant leading edge gives the high first positive peak in the waveform whereas the blant trailing edge gives the high second positive peak.

Figure 10 shows the comparison of computed waveform between two airfoils keeping the same lift and thickness ratio. Supercritical airfoil fits the design principle because the loading noise (p_2) was reduced by the flat chordwise pressure distribution and the positive peak of loading noise was delayed to cancel the negative peak of thickness noise (p_1). It was shown that this supercritical airfoil presents lower total noise level (p) compared with the NACA 0011 airfoil. The respective pressure distributions are shown in Figure 11.

In Figure 10, the observer times when the leading edge or the trailing edge passes the rotor azimuthal angle $\psi=90°$, where the most intense source is generated and also the most dynamically the integral region is elongated are shown. The interval of these two times can be estimated roughly from equation (13) as about $c_h/R\Omega$.

Here are some examples of computed results of peak to peak pressure amplitude as functions of observer position, disk loading, or airfoil sectional shape. Figure 12 shows the noise level as a function of observer elevation angle. Thickness noise (p_1) radiate most strongly in the rotor plane ($\delta=0°$) whereas the loading noise (p_2) radiate most strongly about 20° under the rotor plane ($\delta=-20°$). Though both noise components radiate almost symmetrically about the rotor plane, the directivity of total noise has lost the symmetric character. This is caused by the difference

of the effect of phase shift of two components which is expressed here by $p/(p_1+p_2)$ as a chain line. The smaller the value of $p/(p_1+p_2)$ becomes, the more the phase shifting is effective in noise reduction. When the observer is above the rotor plane, the noise level is low because the first positive peak of thickness noise is canceled by the negetive peak of loading noise. The negative peak of thickness noise is also canceled a little by the positive value of loading noise.

Figure 13 shows the noise level as a function of thrust coefficient over solidity, c_T/σ. The phase shifting effect is effective at high c_T/σ, because the dipole source distribution is resembling to the monopole source distribution at low angle of attack whereas the dipole source distribution is favourable at high angle of attack.

Figure 14 through Figure 17 show the parametric study of the effect of airfoil or sectional shape on noise level. Airfoils studied are all in NACA-4 digit series, whereas thickness ratio, maximum thickness position, leading edge radius, or camber are parametrically changed. Rotor thrust is equated as $c_T/\sigma=0.091$ through all examples.

In these parameters, the influence of camber is most remarkable on the phase shifting effect. An adequate amount of camber realizes a favourable dipole source distribution as in the case of high angle of attack as stated before. Small leading edge radius and maximum thickness near mid-chord are preferable but they have little influence on phase shifting. Making blade tip thinner will be very effective in reducing thickness noise.

6 CONCLUSION

The concept of low noise airfoil design by controling the chordwise source intensity distribution of each noise component was shown. It was concluded that a flat-top lift distribution which could be realized by well designed camber or taking moderate angle of attack was favourable because the big negative peak of monopole noise might be canceled by the delayed positive peak of dipole noise in waveform. Here although only monopole source and dipole source are discussed, this concept for noise reduction is effective for the case including other noise source as quadrupole. Solving an inverse problem to design an optimum blade sectional shape might be the next step.

REFERENCES

1) Nakamura, Yoshiya and Azuma, Akira : An Improved Method for Calculating the Thickness Noise. Presented at the International Specialists Symposium on Helicopter Acoustics, May 1978.

2) Azuma, Akira and Kawachi, Keiji : Local Momentum Theory and Its Applications to the Rotary Wing. AIAA Paper No.75-865, 1975, or Journal of Aircraft, Vol.16, No.1, 1979, 6-14.

3) Moriya, Tomijiro : Theory of Airodynamics. Baifukan, August 1959, 95-111.

TABLE I

Dimensions:

Rotor radius; R, m	5.0
Blade cut out; R_0, m	0.7
No. of blades; B	2
Blade chord; c_h, m	0.4
Blade thickness ratio; h_{max}/c_h	0.10
Airfoil section	NACA 4-digit series
Thrust coefficient; c_T/σ	0.091

Operating Conditions:

Forward speed; V_1, m/sec	0 or 55.08 (μ=0.18)
Tip Mach number; M_T	0.9

Observer:

Observer distance; r, m	50
Observer elevation angle; δ,deg	-30

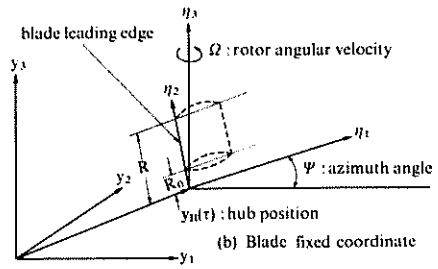

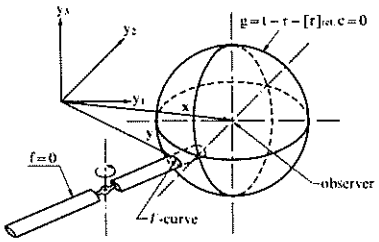

Fig.1 Geometric Relations

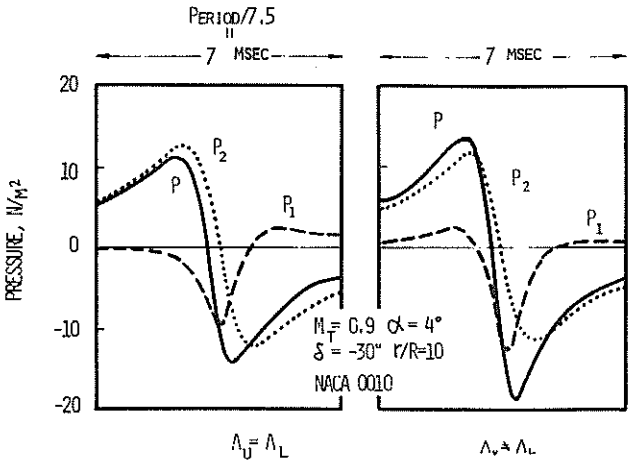

Fig.3 Effect of Assuming $\Lambda_u = \Lambda_L$ on Waveform

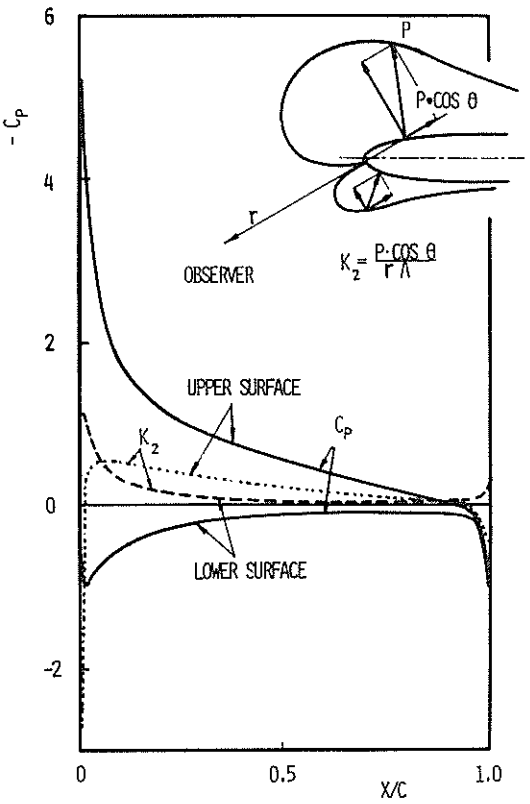

Fig.2 Chordwise Pressure and Dipole Distribution of NACA 0011

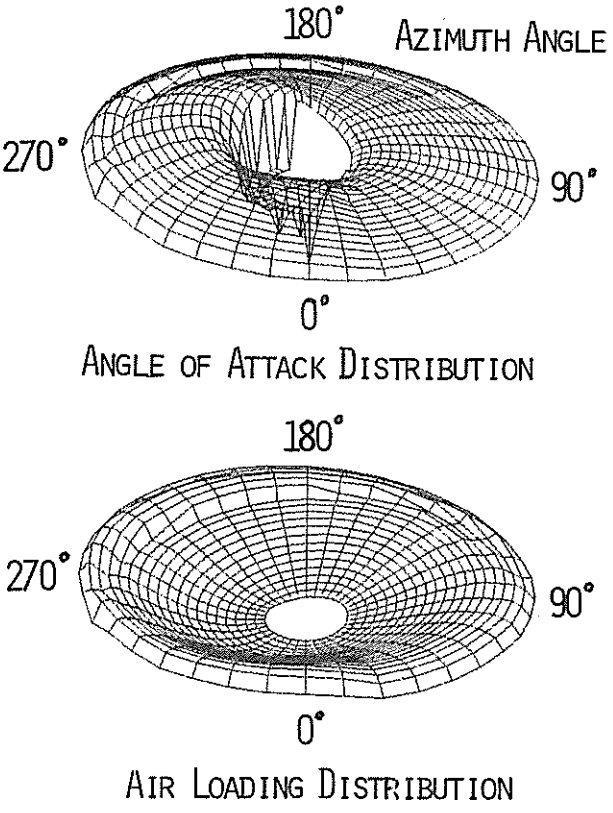

Fig.4 Blade-Vortex Interaction Effect Computed by LMT Program (c=0.8)

μ=0.18, c_T/σ=0.084, B=4,
M_T=0.59, θ_T=-8
(NASA TN-D 1637)

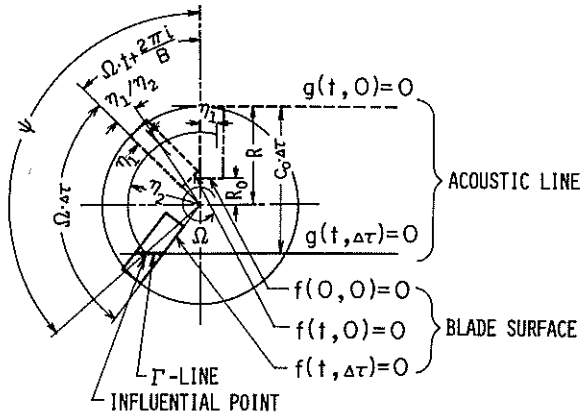

$$F=\cos\alpha(\eta_2\cos\psi-R)\Omega/c_0+\psi-(\Omega t+2\pi i/B-\eta_1/\eta_2)=0$$

Fig.5 Geometric Arrangements of an Influential Point

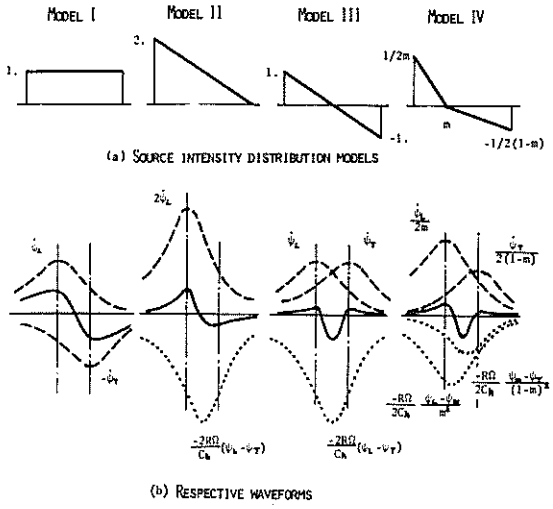

Fig.6 Source Distribution and Waveform

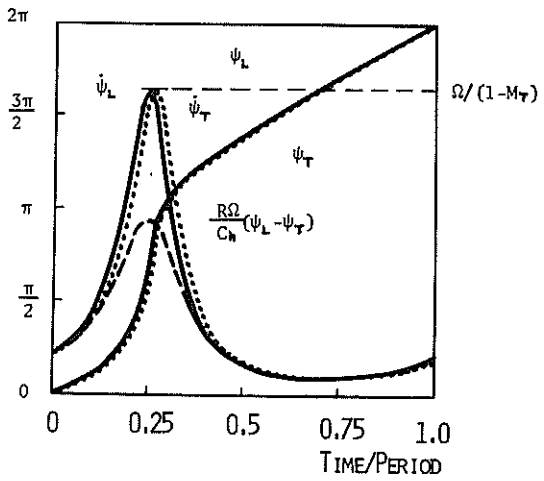

Fig.7 Retarded Time Factors

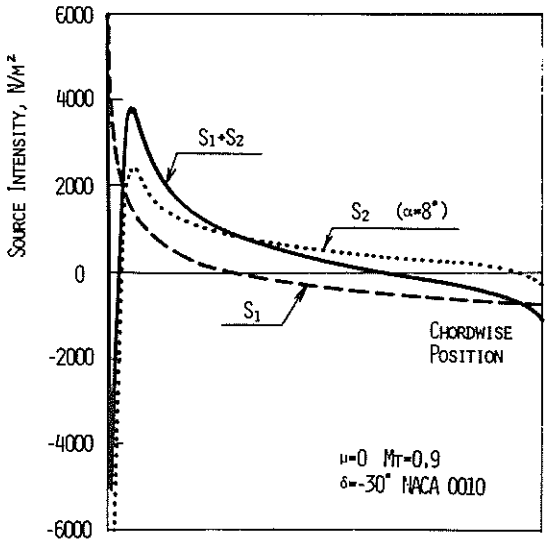

Fig.8 An Example of Actual Chordwise Source Intensity Distribution

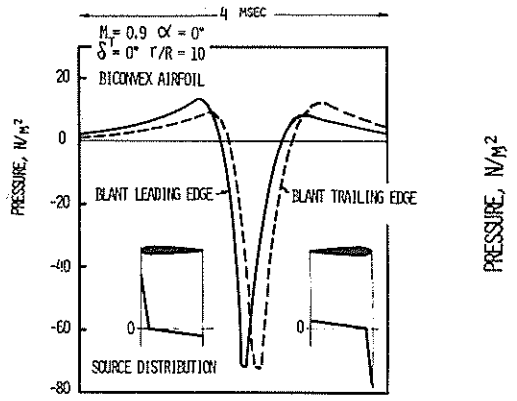

Fig.9 Effect of Maximum Thickness Position on the Waveform of Thickness Noise

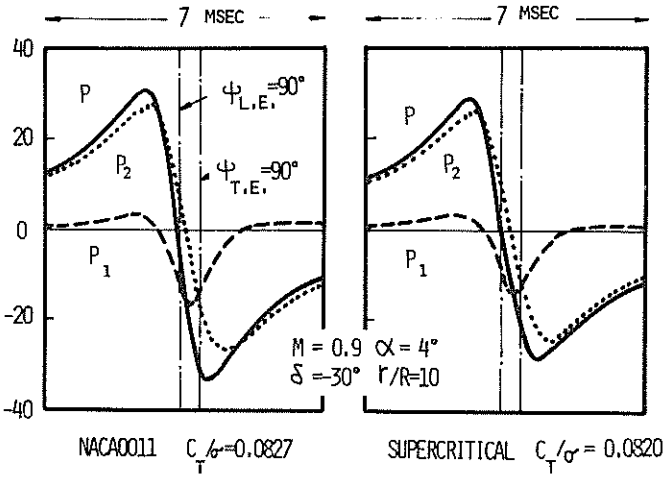

Fig.10 Comparison of Waveform between Two Airfoils

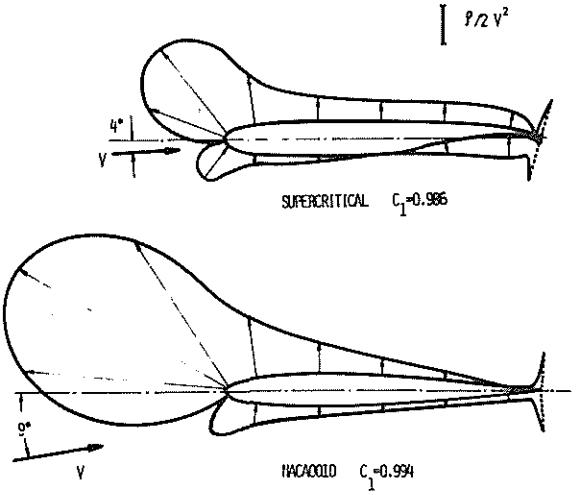

Fig.11 Comparison of Pressure Distribution between Two Airfoils Having the Same Lift Coefficient

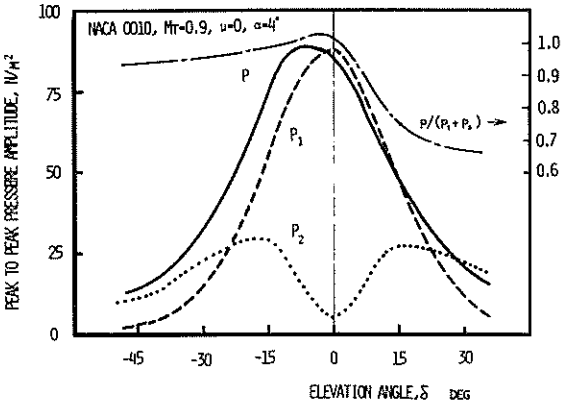

Fig.12 Noise Level vs Elevation Angle

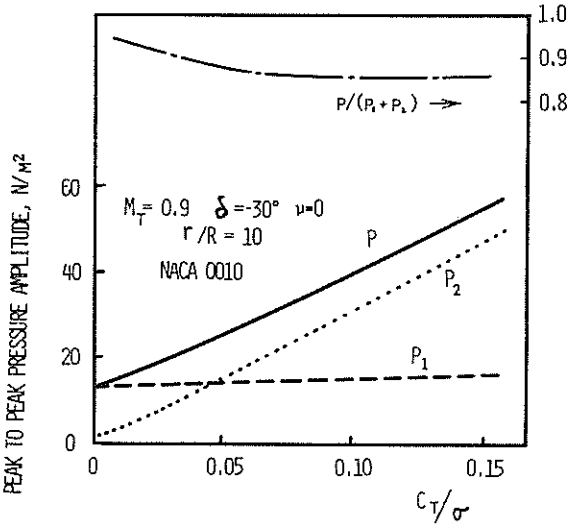

Fig.13 Noise Level vs Thrust

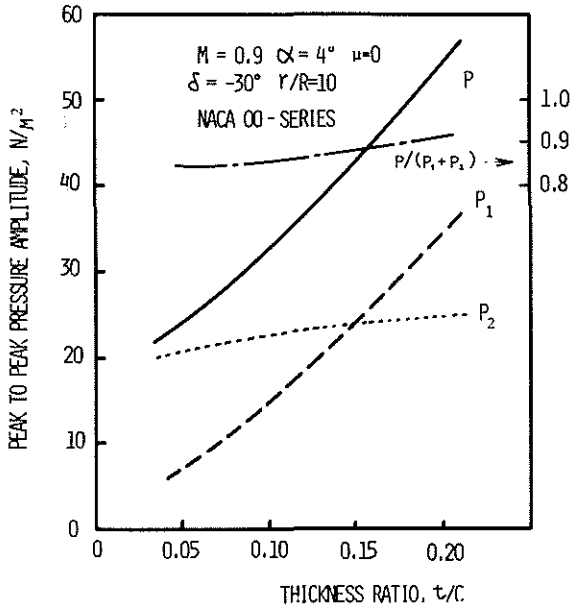

Fig.14 Noise Level vs Blade Thickness

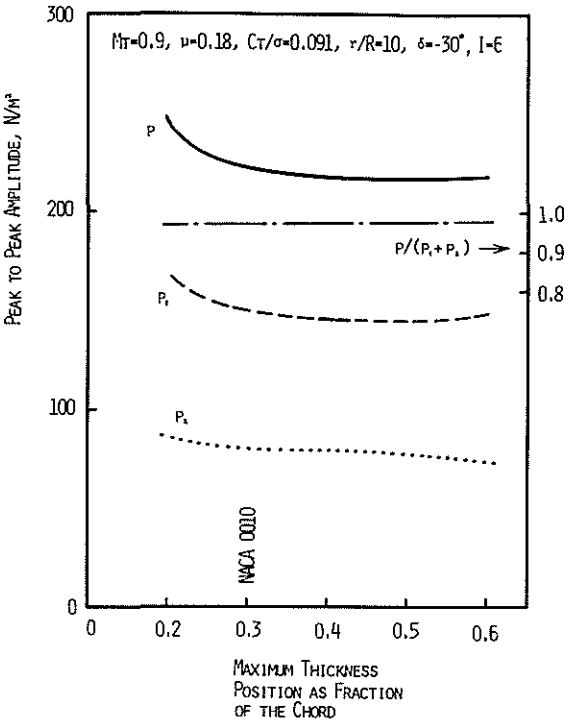

Fig.15 Noise Level vs Max. Thickness Position

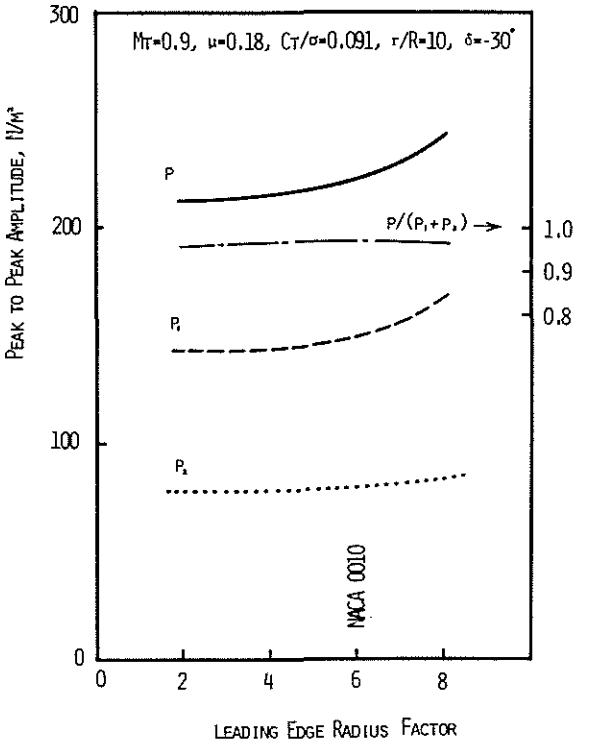

Fig.16 Noise Level vs Leading Edge Radius

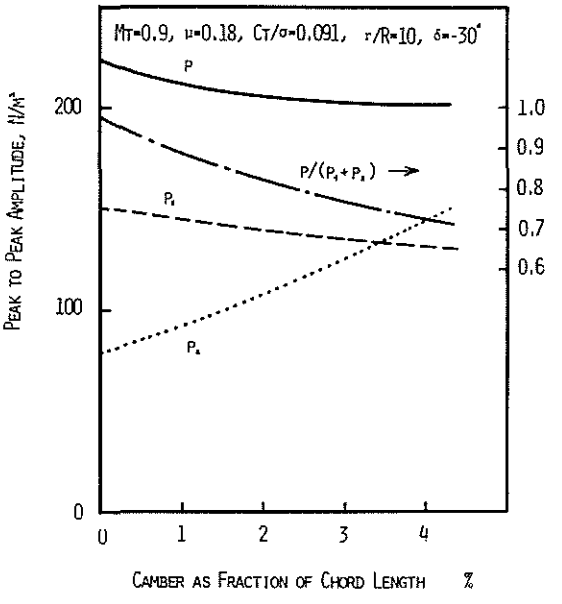

Fig.17 Noise Level vs Camber